Defects at the Nanoscale Impact Contact Line Motion at all Scales

Hugo Perrin,[1] Romain Lhermerout,[2] Kristina Davitt,[2] Etienne Rolley,[2] and Bruno Andreotti[1]
[1]*Physique et Mécanique des Milieux Hétérogènes, UMR 7636 ESPCI -CNRS, Université Paris-Diderot, 10 rue Vauquelin, 75005 Paris, France*
[2]*Laboratoire de Physique Statistique, Ecole Normale Supérieure, UPMC Université Paris 06, Université Paris Diderot, CNRS, 24 rue Lhomond, 75005 Paris, France*
(Received 15 November 2015; revised manuscript received 19 February 2016; published 2 May 2016)

The contact angle of a liquid drop moving on a real solid surface depends on the speed and direction of motion of the three-phase contact line. Many experiments have demonstrated that pinning on surface defects, thermal activation and viscous dissipation impact contact line dynamics, but so far, efforts have failed to disentangle the role of each of these dissipation channels. Here, we propose a unifying multiscale approach that provides a single quantitative framework. We use this approach to successfully account for the dynamics measured in a classic dip-coating experiment performed over an unprecedentedly wide range of velocity. We show that the full contact line dynamics up to the liquid film entrainment threshold can be parametrized by the size, amplitude and density of nanometer-scale defects. This leads us to reinterpret the contact angle hysteresis as a dynamical crossover rather than a depinning transition.

DOI: 10.1103/PhysRevLett.116.184502

When a liquid drop spreads on a solid surface, shear flow in the meniscus creates viscous dissipation that causes the apparent contact angle θ_M at the macroscopic scale to shift from its static value θ_Y [1]. Because of the divergence of the viscous shear stress at the contact line, each decade of length scale down to the molecular size contributes equally to this dissipation. This problem has been thoroughly studied and its understanding has now reached a consensual agreement [2,3]. Integrating the meniscus profile from the molecular scale, where the microscopic contact angle θ_μ is assumed to be at equilibrium, up to the macroscopic boundary condition—which can be a reservoir, a drop, or a channel—provides a relation between θ_M and the capillary number $\mathrm{Ca} \equiv \eta U/\gamma$, which is the contact line velocity U normalized by the liquid-vapor surface tension γ and the liquid viscosity η [4,5]. This purely hydrodynamic approach fails to account for the logarithmic time relaxation of the contact angle frequently observed at low velocity [6–9]. In a seminal paper by Blake [10], it was first suggested that even the molecular discreteness of a solid could generate a rugged energy landscape [11] and cause the contact line dynamics to be thermally activated. Kramers theory predicts that thermal activation yields a relation between the contact line velocity and the microscopic contact angle θ_μ of the form

$$|\mathrm{Ca}| \propto \exp\left[\frac{\gamma \ell^2 |\cos\theta_\mu - \cos\theta_Y|}{k_B T}\right], \qquad (1)$$

where k_B is the Boltzmann constant, T the temperature, and ℓ a characteristic length of activation [12]. Direct experimental evidence of this temperature-dependent activation over nanoscale defects present on the solid surface was obtained by [6]. It has also been proposed that the pinning and depinning events at work in the activated motion of the contact line could also be responsible for the contact angle hysteresis [13–15].

Contact angle dynamics is, thus, a demanding multiscale problem. Despite several attempts [8,9,16,17], this phenomenon is lacking a unifying picture capable of accounting for both viscous dissipation (acting at all scales) and activated dynamics (acting at the nanometer scale). Furthermore, thermal activation has neither been rigorously related to the defects of the solid surface, nor to the wetting hysteresis.

Here, we propose a unified description that combines a hydrodynamic description of the liquid flow at large scales and a Langevin description of the contact line motion at the nanoscale. We have studied the classic dip-coating geometry both theoretically and experimentally [9,18–23], where an apparently flat plate is pulled out of or dipped into a liquid bath at a fixed velocity. As shown by the fit in Fig. 1(a), our multiscale approach accounts for the entire range of dynamics. We are able to achieve a quantitative description over five decades in Ca up to the film entrainment threshold [18,20–24] by adjusting the mean characteristics of the nanoscale defects (density, amplitude, and spacing) that are inevitably present on the plate. Finally, we show that the contact angle hysteresis, which is usually thought to be related to the critical mechanical force needed to unpin the contact line from the defects [25], is, instead, related to a crossover between a low-velocity activated regime and a high-velocity viscous regime.

Framework.—We consider a plate covered with nanoscale heterogeneities that is withdrawn vertically and at constant velocity U from a liquid bath. Because of transient

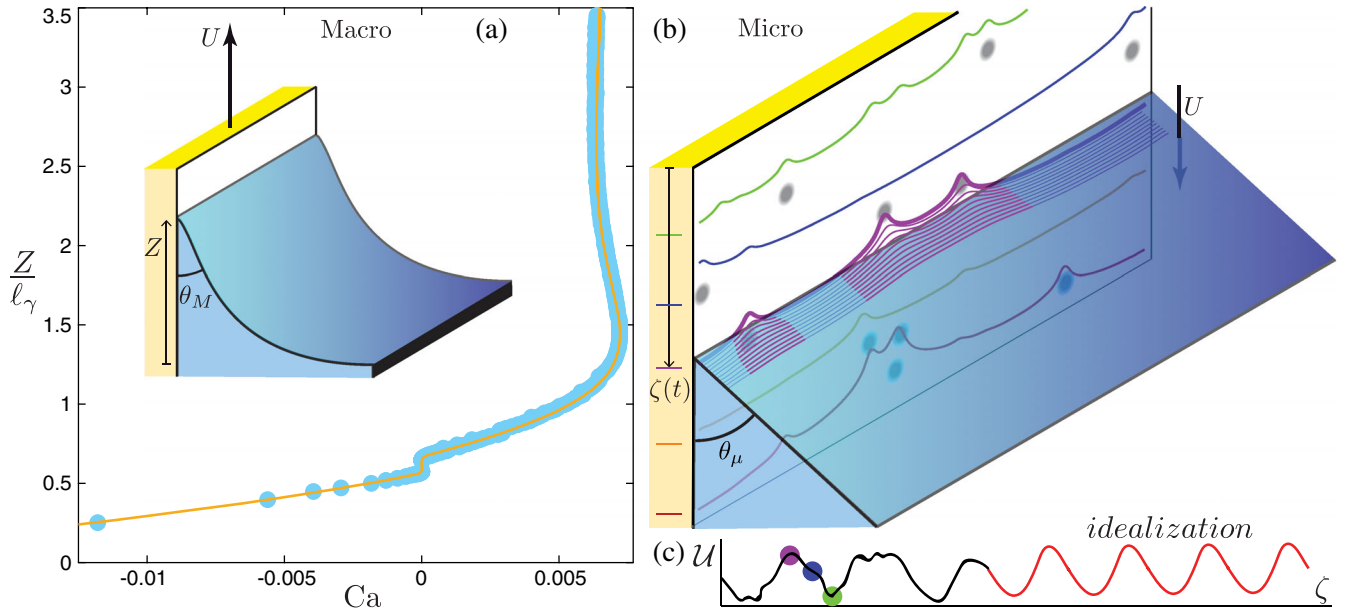

FIG. 1. (a) Height Z of the contact line as a function of the capillary number Ca, in the limit $\dot{Z} \to 0$ (Z is rescaled by the capillary length $\ell_\gamma = \sqrt{\gamma/\rho g}$ where ρ is the liquid density and g the acceleration of gravity). Circles: experimental data. Solid line: theory. Inset: schematic of the dip-coating experiment in the frame of reference of the bath. (b) Schematic of the contact line deformation over defects in the frame of reference of the plate. (c) Schematized energy landscape along the reaction path. Left: realistic. Right: idealization.

pinning on defects, the contact line as well as the entire liquid-vapor interface are distorted and explore many disordered configurations when the plate is moved, as schematized in Fig. 1(b). These configurations are not directly observable, rather, our aim is to understand how heterogeneities and thermal noise impact measurable averaged properties of the interface such as the capillary rise Z.

In order to develop a statistical description of the contact line, we assume that the fluctuations around the average are small enough to remain in the linear regime and perform a modal decomposition of the interface shape. First, we consider the zero mode, which is invariant along the x direction (transverse to the direction of motion) and average it over microscopic configurations. This average interface is controlled by viscous, capillary, and gravitational forces only. The effect of disorder on the plate is embedded in the boundary condition at the plate: the microscopic contact angle θ_μ. The effect of thermal fluctuations is hidden in the liquid parameters γ and η. The average shape can be accurately described using hydrodynamics in the lubrication approximation extended to large slopes [26]. This allows one to remove the viscous dissipation associated with the zero mode from the measured $Z(\mathrm{Ca})$ and to deduce the contact angle at the nanoscale, $\theta_\mu(\mathrm{Ca})$. The effect of defects present on the plate and the viscous dissipation of higher order modes are embedded in the relation Ca vs θ_μ.

Next, we consider fluctuations of the interface around the zero mode as well as variations in time of the mean contact line position $\zeta(t)$. We assume that heterogeneities are able to pin the contact line locally over a length significantly larger than the atomic size so that the interface can still be described in the framework of continuum hydrodynamics. The time scale of the fluctuations of the instantaneous position of the contact line, written as $\zeta(t) + \epsilon(x,t)$, with $\langle \epsilon \rangle = 0$, is much smaller than the relaxation time of the macroscopic profile which sets the nanoscale contact angle θ_μ: the contact line is, thus, driven at a constant force per unit length $\gamma(\cos\theta_\mu - \cos\theta_Y)$. The goal is, then, to compute the time-averaged drift velocity $U = \langle \dot{\zeta} \rangle$ of the mean instantaneous contact line position $\zeta(t)$ when the line is submitted to a constant force. To account for thermal noise, we make use of reaction-rate theory. Following reaction-path theory [27,28], we reduce the full dynamics of $\epsilon(x,t)$ to the dynamics of the single reaction coordinate ζ assuming that all other degrees of freedom relax much faster to the minimal free energy at fixed ζ. This reaction coordinate, therefore, evolves in an effective random energy landscape $\mathcal{U}(\zeta)$ which has multiple valleys and barriers. By effective, we mean that it originates from the surface heterogeneities but also accounts for the relaxation of all other degrees of freedom besides ζ. The dissipation is the final ingredient needed to write a Langevin equation for ζ. Viscous dissipation associated with the stationary motion of the zero mode has already been taken into account, and it sets the value of the applied force through θ_μ. However, fluctuations of the interface are responsible for an extra dissipation, which leads to a friction force of the form $-\beta\eta\dot{\zeta}$. β is a dimensionless function of ζ which can be calculated in the lubrication approximation [29]. Finally, the Langevin equation governing the motion of the contact line reads

$$\beta\eta\dot{\zeta} = \gamma(\cos\theta_\mu - \cos\theta_Y) - \frac{d\mathcal{U}}{d\zeta} + \sqrt{\frac{2\beta\eta k_B T}{\lambda}}\mathcal{W}(t), \quad (2)$$

where $W(t)$ is a noise obeying the normalization condition: $\langle \mathcal{W}(t)\mathcal{W}(t')\rangle = \delta(t-t')$.

Obtaining θ_μ from the experiment.—The dip-coating experiment illustrated in the inset of Fig. 1(a) is performed in a silicon oil (Rhodorsil V100) composed of chains of $\simeq$150 monomers of length $\simeq$0.3 nm. The molecular size, given by the Gaussian radius, is equal to $\ell_\mu \simeq 3.6$ nm. The viscosity and surface tension under experimental conditions are $\eta = 116$ mPa · s and $\gamma = 23$ mN · m^{-1}. Similar results have been obtained using V50 ($\eta = 54$ mPa · s). The plate is a piece of silicon wafer coated with a layer of fluoropolymer FC725 (3M) approximately 0.5 μm thick. The plate velocity U is controlled by a translation stage and varied between 1 μm · s^{-1} and 4 mm · s^{-1}. The dynamics is obtained by analyzing transients [22], which allows us to go beyond the entrainment threshold (which occurs here at $\mathrm{Ca} = 7.2 \times 10^{-3}$). The average height Z with respect to the bath is determined from a front-view image (25 Hz CCD camera) of the plate, in the limit of vanishing $\dot{Z}$ (Fig. 1). Using a subpixel correlation technique, we achieve a precision of 1 μm. Variations in the bulk liquid bath level due to the excluded volume, which results from the finite thickness of the wafer, are detected using the reflection of a sharp tip from the surface of the bath. The microscopic contact angle $\theta_\mu(\mathrm{Ca})$, defined at the scale ℓ_μ, is deduced from the measurements of $Z(\mathrm{Ca})$ using lubrication equations extended to arbitrary slopes [26,29].

The resulting curve of $\cos\theta_\mu$ vs Ca is displayed in Fig. 2. At first approximation, it shows a nearly logarithmic dependance of the form given in Eq. (1). This is the signature of a thermally activated process. The best fit to Eq. (1) gives a slightly different activation length in the advancing ($\ell = 7.6$ nm) and receding ($\ell = 5.9$ nm) directions.

For a given height of the contact line, the macroscopic contact angle θ_M can be properly defined from the capillary rise using asymptotic matching. Far from the contact line, the influence of both viscosity and surface heterogeneities are negligible in front of gravity and capillarity, and therefore, the shape of the interface becomes asymptotically that of a static meniscus whose macroscopic contact angle with the plate is, nonetheless, selected by small-scale processes. Contact angle dynamics are commonly reported as $\cos\theta_M$ rather than Z. Figure 2 shows the $\cos\theta_M$ which has been obtained from the experimentally measured Z using the capillary rise. It can be seen that θ_μ and θ_M coincide at small capillary numbers, which implies that the viscous dissipation of the zero mode is negligible and that the surface disorder, whose influence is characterized by θ_μ, provides the dominant dissipative process in this region of the dynamics.

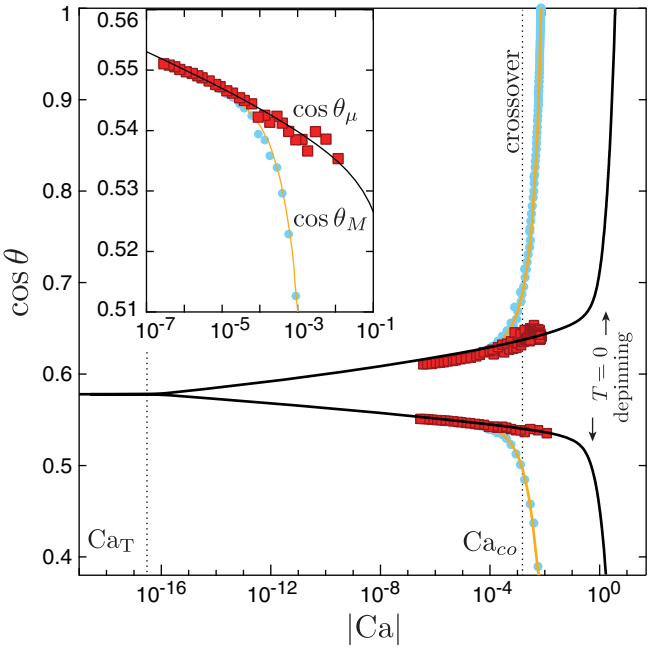

FIG. 2. Cosine of the free surface angle as a function of the capillary number Ca. Circles: experimental macroscopic angle $\cos\theta_M = (Z/\ell_\gamma)\sqrt{1 - 0.25(Z/\ell_\gamma)^2}$. Squares: experimental microscopic angle $\cos\theta_\mu$. Solid lines: theory for the microscopic angle and for the macroscopic angle. The depinning thresholds at zero temperature are indicated by arrows. Inset: close-up of the advancing branch ($\mathrm{Ca} < 0$).

Solving the Langevin equation.—Now, we want to use the Langevin equation to derive the dynamics of the microscopic contact angle. To this aim, we need to build the free energy $\mathcal{U}(\zeta)$ from the defect properties. For simplicity, we consider a periodic series of defects of wave number $q = 2\pi/\lambda$ along both directions of the surface. Following Joanny and de Gennes [13], in the limit of small deformation, we consider that the contact line can be divided into independent pieces of length λ and evaluate the effect of a single defect of size d. This can be seen as a mean-field approximation that models an effective defect and a typical distance between defects of λ. The total free energy $\mathcal{U}$ per unit length contains two contributions: the solid surface-tension landscape, assumed to be composed of Gaussian defects, and the disturbance of the liquid surface, which results in an elasticlike restoring force. From the average position ζ of the contact line, the position ψ of the contact line on the defect, and the dimensionless defect amplitude h, we write the density of free energy as the sum of a contribution from the defects $\sqrt{(\pi/2)}\gamma h d\,\mathrm{erf}(\psi/d\sqrt{2})$ and of a contribution from the liquid-vapor interface, written as $\frac{1}{2}\gamma\kappa q(\zeta-\psi)^2$, where $\kappa \sim \sin^2\theta_Y/[2\ln(\lambda/d)]$ is a dimensionless spring constant [13]. Following reaction-rate theory, for a given value of the average contact line position ζ, the position of the contact line on the defect $\psi(\zeta)$ is selected by minimizing this free energy with respect

to ψ [29]. One obtains the energy landscape $\mathcal{U}(\zeta)$ represented in Fig. 1(c).

The average drift velocity $U = \langle\dot{\zeta}\rangle$ is then obtained by numerical integration of the Langevin equation. The model has four physically meaningful parameters, θ_Y, h, λ, and d, which determine the different characteristics of the curve $\cos\theta_\mu$ vs Ca (Fig. 2). θ_Y is the contact angle at vanishing velocity. λ governs the typical slope far below the depinning transition where the dynamics is logarithmic. The asymmetry between the advancing and receding directions is controlled by $\sim h\lambda/d$. Finally, $h\sqrt{\lambda/d}$ controls the location of the depinning point and of the velocity Ca_T, below which the system is close enough to thermal equilibrium to give a linear relation between the force $(\cos\theta_\mu - \cos\theta_Y)$ and the velocity Ca.

Discussion.—The best fit to the data, therefore, provides a determination of the four parameters. Figure 1(a) shows that this minimal model fits the entire range of experimental data over all of the regimes. The wettable defect diameter $d \simeq 2.5$ nm is significantly smaller than the distance $\lambda \simeq 18$ nm between defects. Under these conditions, the contribution of the contact-line "elasticity" to the energy $\mathcal{U}(\zeta)$ is important: the maximum deformation of the contact line $(\zeta - \psi)$ is relatively large and induces a ratchetlike effect [29], which explains the asymmetry between the advancing and receding directions. The amplitude $h = 0.14$ is low enough to give a single valued function $\mathcal{U}(\zeta)$ (Fig. 1) so that, for a given average position ζ of the contact line, there is a unique position $\psi(\zeta)$ on the defect. In this situation, where the heterogeneities are termed "weak," advancing and receding contact lines pass by the same microscopic configuration at a given location ζ.

The model also predicts the relation between $\cos\theta_\mu$ and Ca in the limit of vanishing temperature for the same four fit parameters. This can be seen from Eq. (2), where for vanishing temperature ($T = 0$) the contact line is at equilibrium ($\dot{\zeta} = 0$) as long as the driving force $\gamma(\cos\theta_\mu - \cos\theta_Y)$ is within the range of the force $d\mathcal{U}/d\zeta$. The depinning angles ($\Theta_r \simeq 47.8°$ and $\Theta_a \simeq 58.4°$), indicated by arrows in Fig. 2, have been determined from the extremal values of $d\mathcal{U}/d\zeta$ [29]. This range corresponds to a truly static contact angle hysteresis, which applies only for vanishing temperature. In this case, between these angles, the contact line is pinned, and beyond them, the velocity asymptotically increases linearly with $\cos\theta_\mu$. As seen in Fig. 2, the depinning transition (near $\mathrm{Ca} = 1$) is blurred at finite temperature, but its presence still has a strong effect on the dynamics of θ_μ. Here, the depinning transition within the thermally activated regime can not be reached experimentally.

The description we propose here accounts for the full range of contact line dynamics and, therefore, must also describe the so-called contact angle hysteresis commonly seen when liquid drops move on real solids. The measured amplitude of the hysteresis has, so far, been linked to the location of the depinning transition. However, it is clear above that, in practice, the depinning transition is not reached. To explain this, one must realize that a typical procedure for measuring the hysteresis involves inflating or deflating a drop and waiting a certain time until the drop edge is determined to cease moving. This pseudoequilibrium condition depends on the apparatus resolution and in practice corresponds to waiting only for the first fast phase of relaxation. The hysteresis in this case coincides with a crossover between the high Ca regime where large-scale viscous dissipation dominates, and a low Ca regime where dissipation occurs mainly at the defect scale. For practical purposes, we can define a point of crossover between regimes as the capillary number $\mathrm{Ca}_{\mathrm{co}}$ for which the difference between $\cos\theta_M$ in the advancing and receding directions is twice the difference between $\cos\theta_\mu$. For this system, we find $\mathrm{Ca}_{\mathrm{co}} = 1.5 \times 10^{-3}$ and an advancing contact angle of $\theta_\mu^r \simeq 50.4°$ for a receding contact angle of $\theta_\mu^a \simeq 57.3°$ (Fig. 2). So, $(\theta_\mu^a - \theta_\mu^r)$ would quantify the hysteresis measured by standard procedures. Except when strong macroscopic defects are present on the solid surface, such a "hysteresis" is not directly connected to the maximum pinning force of the defects, which is measured by $(\Theta_a - \Theta_r)$.

Finally, we comment on the difference between our approach and the static picture proposed by Joanny and de Gennes. In the latter picture, weak defects do not trigger multistability with respect to ψ, at a constant mean contact line position ζ: there is no hysteresis for the microscopic configuration of the contact line when ζ is varied in one direction or the other [11,13,30]. Here, we use a dynamic description where the contact line position ζ becomes a dynamic variable [31,32]. Multiple local minima (and, therefore, hysteresis) appear when ζ is moved and no longer imposed. The model we propose here is appropriate as long as the defects are small enough such that the deformations of the contact line are smaller than the capillary length, provided that they remain weak. We expect strong heterogeneities to lead to a substantially different behavior. In this case, the depinning transition may occur before the viscous crossover if the disorder-induced dissipation becomes larger than the viscous dissipation associated with the overall motion of the contact line. Future experiments will have to test this scenario, in particular, using surfaces whose heterogeneities are controlled in order to investigate the transition from weak to strong heterogeneities.

This work is supported by ANR SMART and REALWET. B. A. acknowledges support from the IUF. We thank J. H. Snoeijer for fruitful discussions.

[1] P.-G. de Gennes, F. Brochard-Wyart, and D. Quere, *Capillarity and Wetting Phenomena: Drops, Bubbles, Pearls, Waves* (Springer, New York, 2004).

[2] D. Bonn, J. Eggers, J. Indekeu, J. Meunier, and E. Rolley, Rev. Mod. Phys. **81**, 739 (2009).
[3] J. H. Snoeijer and B. Andreotti, Annu. Rev. Fluid Mech. **45**, 269 (2013).
[4] J. Eggers, Phys. Rev. Lett. **93**, 094502 (2004).
[5] J. Eggers, Phys. Fluids **17**, 082106 (2005).
[6] A. Prevost, E. Rolley, and C. Guthmann, Phys. Rev. Lett. **83**, 348 (1999).
[7] T. D. Blake, in *Wettability*, edited by J. Berg (Marcel Dekker, New York, 1993), Vol. 49, pp. 251–309.
[8] J. G. Petrov and P. G. Petrov, Colloids Surf. **64**, 143 (1992).
[9] P. Petrov and J. Petrov, Langmuir **8**, 1762 (1992).
[10] T. D. Blake and J. M. Haynes, J. Colloid Interface Sci. **30**, 421 (1969).
[11] A. Giacomello, L. Schimmele, and S. Dietrich, Proc. Natl. Acad. Sci. U.S.A. **113**, E262 (2016).
[12] T. D. Blake and J. De Coninck, Eur. Phys. J. Spec. Top. **197**, 249 (2011).
[13] J.-F. Joanny and P.-G. de Gennes, J. Chem. Phys. **81**, 552 (1984).
[14] E. Rolley and C. Guthmann, Phys. Rev. Lett. **98**, 166105 (2007).
[15] K. Davitt, M. S. Pettersen, and E. Rolley, Langmuir **29**, 6884 (2013).
[16] D. Seveno, A. Vaillant, R. Rioboo, H. Adao, J. Conti, and J. De Coninck, Langmuir **25**, 13034 (2009).
[17] M. Ramiasa, J. Ralston, R. Fetzer, R. Sedev, D. M. Fopp-Spori, C. Morhard, C. Pacholski, and J. P. Spatz, J. Am. Chem. Soc. **135**, 7159 (2013).
[18] R. V. Sedev and J. G. Petrov, Colloids Surf. **53**, 147 (1991).
[19] R. A. Hayes and J. Ralston, J. Colloid Interface Sci. **159**, 429 (1993).
[20] J. H. Snoeijer, G. Delon, M. Fermigier, and B. Andreotti, Phys. Rev. Lett. **96**, 174504 (2006).
[21] J. H. Snoeijer, B. Andreotti, G. Delon, and M. Fermigier, J. Fluid Mech. **579**, 63 (2007).
[22] G. Delon, M. Fermigier, J. H. Snoeijer, and B. Andreotti, J. Fluid Mech. **604**, 55 (2008).
[23] J. H. Snoeijer, J. Ziegler, B. Andreotti, M. Fermigier, and J. Eggers, Phys. Rev. Lett. **100**, 244502 (2008).
[24] I. Peters, J. H. Snoeijer, A. Daerr, and L. Limat, Phys. Rev. Lett. **103**, 114501 (2009).
[25] A. Rosso and W. Krauth, Phys. Rev. E **65**, 025101(R) (2002).
[26] J. H. Snoeijer, Phys. Fluids **18**, 021701 (2006).
[27] H. A. Kramers, Physica **7**, 284 (1940).
[28] P. Hänggi, P. Talkner, and M. Borkover, Rev. Mod. Phys. **62**, 251 (1990).
[29] See Supplemental Material at http://link.aps.org/supplemental/10.1103/PhysRevLett.116.184502 for details on the lubrication approximation and on the Langevin equation.
[30] M. Delmas, M. Monthioux, and T. Ondarçuhu, Phys. Rev. Lett. **106**, 136102 (2011).
[31] E. Raphael and P.-G. de Gennes, J. Chem. Phys. **90**, 7577 (1989).
[32] C. Caroli and P. Nozières, Eur. Phys. J. B **4**, 233 (1998).